ELSEVIER

Journal of Organometallic Chemistry 573 (1999) 47–59

Journal of Organometallic Chemistry

Synthesis, structure and electrochemical studies of the first mixed-metal clusters with the P–N–P assembling ligands $(Ph_2P)_2NH$ (dppa), $(Ph_2P)_2N(CH_3)$ (dppam) and $(Ph_2P)_2N(CH_2)_3Si(OEt)_3$ (dppaSi)[1]

Isolde Bachert [a], Pierre Braunstein [a,*], Mark K. McCart [a], Fabrizia Fabrizi de Biani [b], Franco Laschi [b], Piero Zanello [b], Guido Kickelbick [c], Ulrich Schubert [c]

[a] *Laboratoire de Chimie de Coordination, UMR 7513 CNRS, Université Louis Pasteur, 67070 Strasbourg Cedex, France*
[b] *Dipartimento di Chimica dell'Università di Siena, Pian dei Mantellini 44, 53100 Siena, Italy*
[c] *Institut für Anorganische Chemie, Technische Universität Wien, Getreidemarkt 9/153, A-1060 Wien, Austria*

Received 23 January 1998

Abstract

Heterometallic triangular palladium–cobalt clusters stabilized by three bridging diphosphine ligands such as $Ph_2PNHPPh_2$ (dppa), $(Ph_2P)_2N(CH_3)$ (dppam), $(Ph_2P)_2N(CH_2)_3Si(OEt)_3$ (dppaSi), or mixed ligand sets $Ph_2PCH_2PPh_2$ (dppm)/dppa, dppm/dppam or dppm/dppaSi have been prepared with the objectives of comparing the stability and properties of the clusters as a function of the short-bite diphosphine ligand used and of making possible their use in the sol–gel process (case of dppaSi). The crystal structure determination of $[CoPd_2(\mu_3\text{-}CO)_2(\mu\text{-}dppam)_3]PF_6$ confirms the triangular arrangement of the metal core, with each edge bridged by a dppam ligand, although disorder problems prevent a detailed discussion of the bonding parameters. Different approaches are given to functionalize the heterometallic clusters: alkylation of the nitrogen atom of co-ordinated dppa ligands or introduction of a third bridging diphosphine in a precursor tetranuclear cluster containing only two bridging diphosphine ligands. In the latter case, it was found that their nature critically determined whether or not the reaction occurred. The diversity of bridging ligands allowed an investigation of their influence on the electrochemical properties of the clusters. By comparison with $[CoPd_2(\mu_3\text{-}CO)_2(CO)_2(\mu\text{-}dppm)_2]^+$ which contains only two assembling ligands, it is generally observed that trinuclear cationic $CoPd_2$ clusters containing three (identical or different) edge-bridging bidentate diphosphine ligands show increased redox flexibility. A notable stabilisation of the metal core is observed when three dppm ligands bridge the metal–metal bonds and $[CoPd_2(\mu_3\text{-}CO)_2(\mu\text{-}dppm)_3]$ reversibly undergoes either a single-step two-electron oxidation or two distinct one-electron reductions. Complexes with the other diphosphines exhibit similar redox behaviour, but the stability of their redox congeners depends upon the nature of the diphosphine: a lower redox aptitude is exhibited by the dppa and dppam derivatives $[CoPd_2(\mu_3\text{-}CO)_2(\mu\text{-}dppa)_3]^+$ and $[CoPd_2(\mu_3\text{-}CO)_2(\mu\text{-}dppam)_3]^+$.

Keywords: Crystal structure; Electrochemical studies; Mixed metal clusters; P–N–P assembling ligands; Short-bite ligands

1. Introduction

Among the various short-bite ligands available for assembling metal centres in bi- or polynuclear metal complexes, bis(diphenylphosphinoamine) ($Ph_2PNHPPh_2$, dppa) is particularly attractive owing to its isoelectronic relationship with the bis(diphenylphosphinomethane) ligand ($Ph_2PCH_2PPh_2$, dppm) which has been more extensively and very successfully used in binuclear and cluster chemistry [1,2]. However, only few heterometallic complexes containing the dppa ligand have been reported ([1]a–c). The greater acidity of the NH proton versus the CH_2 protons may facilitate

* Corresponding author. E-mail: braunst@chimie.u-strasbg.fr

[1] Dedicated to Professor Brian Johnson on the occasion of his 60th birthday in recognition of his outstanding contributions to organometallic and inorganic chemistry, with our best wishes.

0022-328X/99/$ - see front matter
PII S0022-328X(98)00636-6

subsequent functionalization reactions that would require too drastic conditions in the dppm case [2]. Here we report on the synthesis and structure of a series of mixed-metal clusters containing the dppa and the related assembling ligands $(Ph_2P)_2N(CH_3)$ (dppam) and $(Ph_2P)_2N(CH_2)_3Si(OEt)_3$ (dppaSi) obtained by their N-derivatization. Clusters containing the dppaSi ligand represent valuable precursors for the preparation of new materials by the sol–gel process for the covalent incorporation of a mixed-metal cluster into a silica matrix. Heterometallic triangular clusters containing mixed ligand sets have also been prepared by direct incorporation of the second diphosphine ligand and the nature of the precursor clusters has been found to play a critical role.

In spite of the fact that less attention has been paid to the electrochemistry of heteronuclear carbonyl clusters compared with homonuclear clusters, the electrochemical behaviour of triangular heterometallic clusters has received special attention [3,4]. We report here on the redox properties of the heterometallic clusters mentioned above, $[CoPd_2(\mu_3\text{-}CO)_2(\mu\text{-diphosphine})_3]^+$, as a function of the nature of the edge-bridging diphosphine ligands and compare the results with those obtained for $[CoPd_2(\mu_3\text{-}CO)_2(CO)_2(\mu\text{-dppm})_2]$ which contains only two bridging dppm ligands [5].

2. Results and discussion

2.1. Synthetic studies

By analogy with the reactions that led to the first series of heterometallic dppm clusters, and of $[Co_2Pd_2(\mu_3\text{-}CO)_2(CO)_5(\mu\text{-dppm})_2]$ (**1a**) in particular [6], we have reported in a preliminary communication [2] the reaction of $[Pd_2Cl_2(\mu\text{-dppa})_2]$ [7] with two equivalents of $Na[Co(CO)_4]$ in THF (12 h, −78 to 30°C) which resulted in an immediate colour change from orange–yellow to deep blue and green. After filtration to remove NaCl, evaporation of the solvent, washing with ethanol, diethylether and hexane and recrystallization from CH_2Cl_2/pentane, a microcrystalline powder of $[Co_2Pd_2(\mu_3\text{-}CO)_2(CO)_5(\mu\text{-dppa})_2]$ (**1b**) was obtained in 86% yield (Eq. (1)):

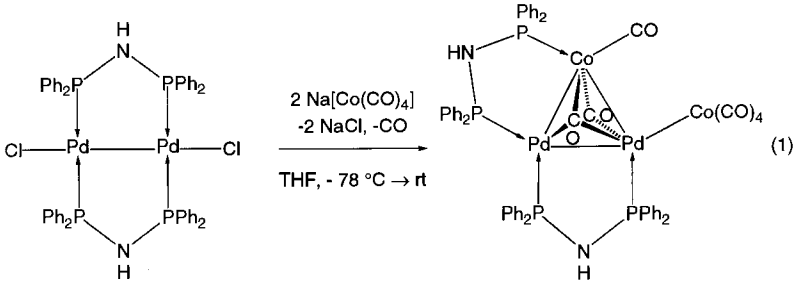

(1)

1b

Analytical and spectroscopic data were fully consistent with the structure shown in Eq. (1) and its similarity to **1a** [2]. The two protons of the amino groups of the co-ordinated dppa ligands of **1b** are non-equivalent and give rise to two broad singlets around δ 6.59 and 6.54 ppm in acetone-d_6 because of coupling to the adjacent phosphorus atoms. Their assignment has been confirmed by exchange with D_2O. The $^{31}P\{^1H\}$-NMR resonances for the Pd-bound P atoms of **1b** appear at δ 51.7, 48.1 and 42.4 (multiplets) whereas the Co-bound P nucleus gives rise to a broad resonance at δ 77.1 owing to the quadrupolar effect of cobalt. These resonances are shifted to lower field compared with those for its dppm analogue **1a**, which is in agreement with the differences of the chemical shifts of the free ligands ([6]a). A discussion of the values of the coupling constants is more difficult and has to be based on a comparison with the dppm-containing clusters owing to the lack of data on dppa-containing compounds ([6]a). The small value of 54 Hz for the $J(P^2–P^3)$ coupling is consistent with a *cis* relationship of P^2 and P^3 (the numbering of the phosphorus atoms is shown in the Experimental Section). Although $J(P^1–P^4)$ is a three bond coupling, its relatively large value of 166 Hz is in agreement with a *transoid* $P^1–Pd–Co–P^4$ arrangement. The $J(P^1–P^2)$ coupling of 154 Hz is consistent with two P atoms of the same diphosphine ligand. The coupling constant $J(P^3–P^4)$ was not resolved and should be viewed as the sum of a two bond coupling constant (through the dppa bridge) and a three bond coupling constant (through the Pd–Co bond): $J(P^3–P^4) = |^2J(P^3-P^4) + {}^3J(P^3-P^4)|$. An opposite sign for these two components could account for the small value of $J(P^3–P^4)$ [8]. To the best of our knowledge, the only other reported cluster compounds containing dppa ligands are the homometallic complexes $[M_3(\mu\text{-}X)_2(\mu\text{-dppa})_3]X$ (M = Cu, Ag; X = Cl, Br, I) [9].

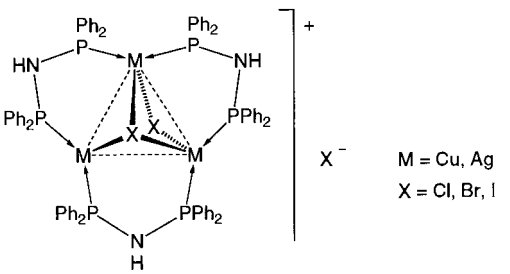

The cationic cluster $[CoPd_2(\mu_3\text{-}CO)_2(\mu\text{-}dppa)_3][PF_6]$ (**2b**) was prepared by reaction of **1b** in THF with one equivalent of dppa in the presence of $[NH_4][PF_6]$ (Eq. (2)). The spectroscopic data are consistent with the cationic cluster containing a mirror plane passing through the cobalt atom and the middle of the Pd–Pd bond [2].

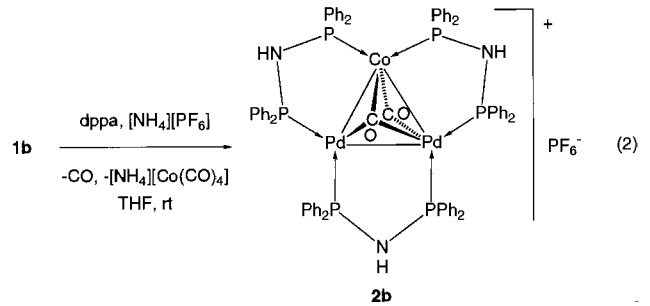

Thus, the amine protons of **2b** give rise to two signals at δ 6.93 and 6.38 ppm, with the signal at δ 6.93 ppm being assigned to the diphosphine bridging the Pd–Pd bond and the other with double intensity to the amine proton of the diphosphines bridging the heteronuclear bonds. This cluster shows three mutliplets in the $^{31}P\{^1H\}$-NMR spectrum at δ 75.9, 41.6 and 40.0 ppm with the resonance for the phosphorus atoms on cobalt being broadened and most downfield shifted. The two signals for the phosphorus atoms on palladium could not be unambiguously attributed.

In order to functionalize cluster **2b**, we reacted a THF solution with excess DBU and then with MeI. The new cluster $[Co_2Pd(\mu_3\text{-}CO)_2(\mu\text{-}dppam)_3][PF_6]$ (**2c**) was obtained in 71% yield (Eq. (3)). We believe that alkylation of all three nitrogen atoms proceeds via successive N–H deprotonation and *N*-alkylation steps rather than through the intermediary of a fully deprotonated, anionic cluster.

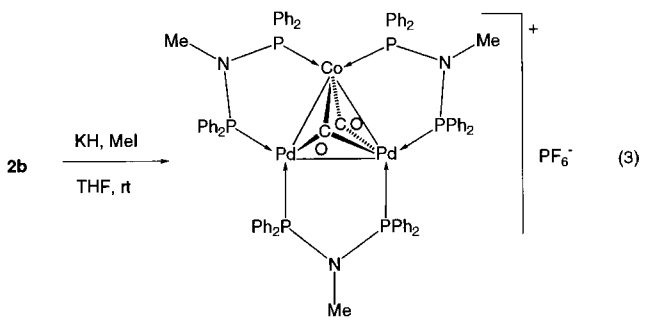

The $^{31}P\{^1H\}$-NMR spectrum of **2c** reveals resonances for three pairs of non-equivalent phosphorus nuclei at δ 100.1 for the two Co-bound P atoms and at δ 67.3 and 63.8 for the two pairs of Pd-bound P atoms. The IR ν(CO) frequency is slightly shifted to lower wavenumbers when compared with **2b**, as expected on the basis of the more electron-donating character of dppam. It is interesting that reaction of the related dppm cluster $[CoPd_2(CO)_2(\mu\text{-}dppm)_3][PF_6]$ (**2a**) with KH followed by alkylation with CH_3I under similar conditions was unsuccessful and only decomposition was observed. If this failure to functionalize the dppm ligands was due to steric factors (12 phenyl groups at the cluster periphery), this explanation should also apply to the dppa cluster **2b**. However, the intrinsically greater acidity of the NH-protons opens the possibility to easily functionalize the bridging ligands. An X-ray diffraction study confirmed the structure drawn for **2c** (see below).

We showed previously [2] that addition of a third functionalized ligand dppaSi to the tetranuclear cluster $[Co_2Pd_2(\mu_3\text{-}CO)_2(CO)_5(\mu\text{-}dppaSi)_2]$ (**1d**) did not allow isolation of $[CoPd_2(\mu_3\text{-}CO)_2(\mu\text{-}dppaSi)_3][PF_6]$. Similarly, reaction of **1d** with one equivalent of dppm or dppa, respectively, did not yield the trinuclear mixed-ligand clusters $[CoPd_2(\mu_3\text{-}CO)_2(\mu\text{-}dppaSi)_2(\mu\text{-}dppm)][PF_6]$ or $[CoPd_2(\mu_3\text{-}CO)_2(\mu\text{-}dppaSi)_2(\mu\text{-}dppa)][PF_6]$, respectively (Eq. (4)).

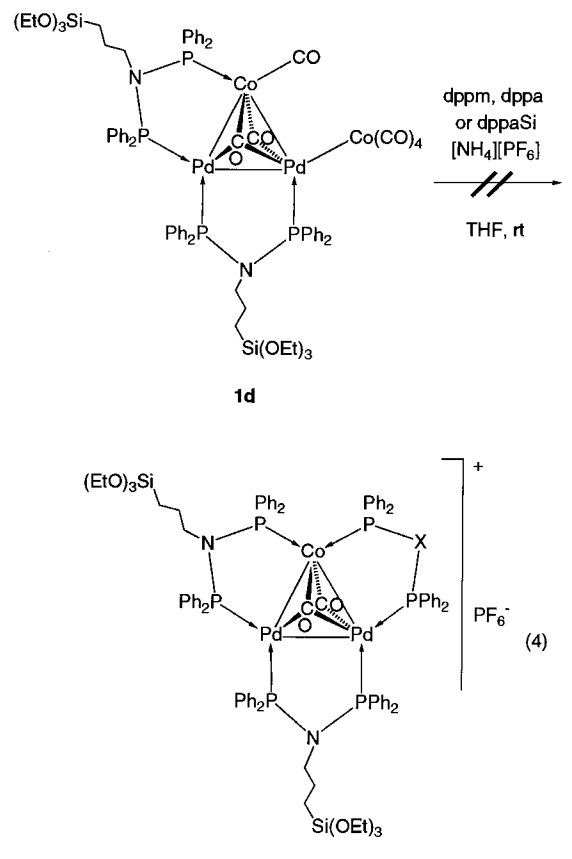

The $^{31}P\{^1H\}$-NMR spectrum of these reaction mixtures revealed different multiplets that could not be assigned to such compounds and pure complexes could not be isolated. Since the triply functionalized, analogous methoxysilyl cluster $[CoPd_2(\mu_3\text{-}CO)_2\{\mu\text{-}(Ph_2P)_2(CH_2)_3Si(OMe)_3\}_3][PF_6]$ (**2d**) has been independently prepared by a different route [2], this failure

cannot be attributed to thermodynamic reasons. Probably the electron donating effect of the N–P π bonding of the co-ordinated dppaSi ligands enhances the electron density of the metal core and reduces the electrophilicity of the palladium and cobalt centres, thus preventing the reactions of Eq. (4).

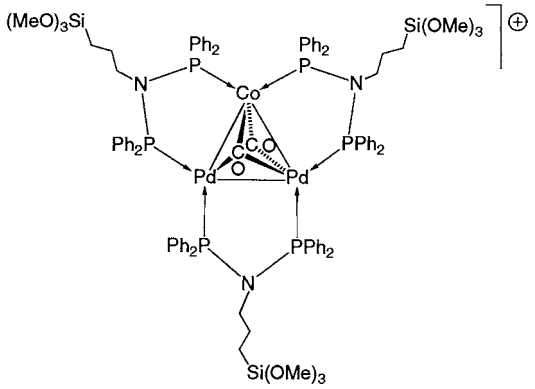

2d

In contrast, the analogous clusters $[Co_2Pd_2(\mu_3\text{-}CO)_2(CO)_5(\mu\text{-dppm})_2]$ (**1a**) and $[Co_2Pd_2(\mu_3\text{-}CO)_2(CO)_5(\mu\text{-dppa})_2]$ (**1b**) are suitable precursors for addition of a functionalized ligand dppaSi. Thus, when these clusters were reacted with one equivalent of dppaSi, under the same conditions as used above for **1d**, the trinuclear mixed-ligand clusters $[CoPd_2(\mu_3\text{-}CO)_2(\mu\text{-dppm})_2(\mu\text{-dppaSi})][PF_6]$ (**3d**) and $[CoPd_2(\mu_3\text{-}CO)_2(\mu\text{-dppa})_2(\mu\text{-dppaSi})][PF_6]$ (**4d**), were obtained, respectively (Eq. (5)).

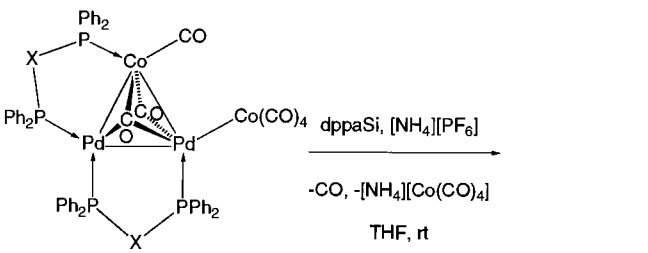

1a X = CH_2
1b X = NH

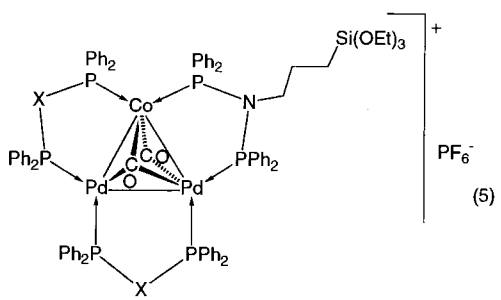

3d X = CH_2
4d X = NH

(5)

The reactions in Eq. (5) show that the ligand dppaSi can be added to the third cluster edge when dppm or dppa are present in the precursor tetranuclear cluster, in contrast to the observations made with **1d**. This indicates the importance of the nature of the bridging diphosphine in the tetranuclear precursors.

The trialkoxysilyl group of clusters **3d** and **4d** allows their use in the sol–gel process for the covalent incorporation of a mixed-metal cluster into a silica matrix [2]. As functionalization of the trinuclear cluster $[CoPd_2(\mu_3\text{-}CO)_2(\mu\text{-dppa})_3][PF_6]$ (**2b**) to give $[CoPd_2(Co)_2(\mu\text{-dppaSi})_3][PF_6]$ (**2d**) has been achieved with the use of an excess of the relatively costly $ICH_2CH_2CH_2Si(OMe)_3$, clusters **3d** and **4d** represent more convenient precursors for subsequent heterogenization.

For comparative purposes, we also prepared triangular clusters containing both dppa and dppm, or dppm and dppam ligands. Mixed ligand sets of the diphosphine type have rarely been introduced in heterometallic systems although this would allow additional tuning of the cluster properties. Thus, reaction of the metalloligated cluster $[Co_2Pd_2(\mu_3\text{-}CO)_2(CO)_5(\mu\text{-dppm})_2]$ (**1a**) with one equivalent of dppa, under conditions similar to those used for the preparation of **3d**, yielded $[CoPd_2(\mu_3\text{-}CO)_2(\mu\text{-dppm})_2(\mu\text{-dppa})][PF_6]$ (**3b**) in 88% yield, which was subsequently methylated to yield $[CoPd_2(\mu\text{-dppm})_2(\mu\text{-dppam})][PF_6]$ (**3c**), using a method similar to that described for the preparation of **2c**. The cluster $[CoPd_2(\mu_3\text{-}CO)_2(\mu\text{-dppm})(\mu\text{-dppa})_2][PF_6]$ (**4a**) was prepared in a manner similar to **2b** from $[Co_2Pd_2(\mu_3\text{-}CO)_2(CO)_5(\mu\text{-dppa})_2]$ (**1b**) and dppm. Spectroscopic IR, ^1H and $^{31}P\{^1H\}$-NMR data for the new complexes with mixed assembling ligands are consistent with the structures shown and the $^{31}P\{^1H\}$-NMR data confirm the presence of six chemically different phosphorus nuclei (Experimental section). Their assignment was performed similarly to those discussed above. The ν(CO) absorption frequencies of the clusters **3b–d** and **4a** are at lower wavenumbers than for the dppm cluster $[Pd_2Co(CO)_2(\mu\text{-dppm})_3][PF_6]$ (**2a**) (1885 cm^{-1}). This result is in agreement with the enhanced electron donating character of the dppa and dppa (R) ligands that induce a shift of the frequency of the carbonyl groups to lower wavenumbers.

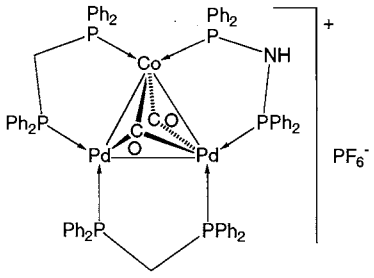

3b

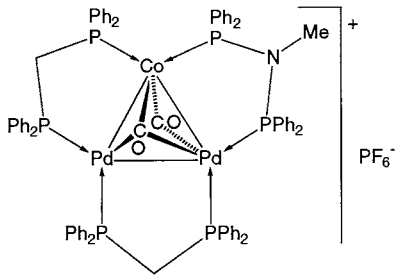

3c

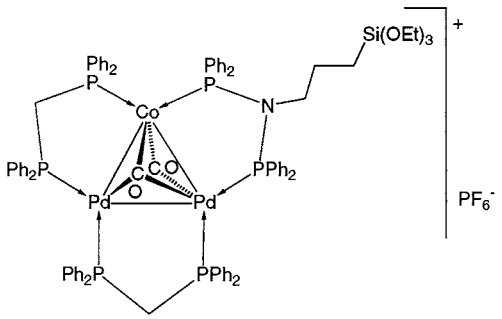

3d

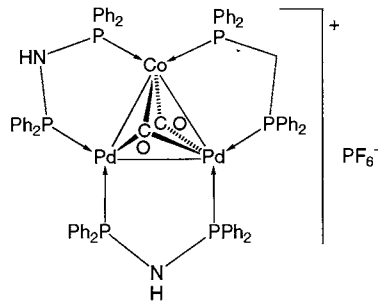

4a

Our results provide an easy entry into mixed-metal clusters containing the dppa ligand and show that the latter can be readily functionalized, in contrast to dppm, to form a wider range of related clusters, including systems with different bridging ligands in well-defined positions. Thus, the synthetic methods employed explain the regioselectivity with which incorporation of the diphosphine ligands occur. The nature of the bridging diphosphine ligands in the tetranuclear precursor cluster plays a decisive role in allowing their transformation into cationic triangular clusters containing three diphosphine bridging ligands. Whereas such

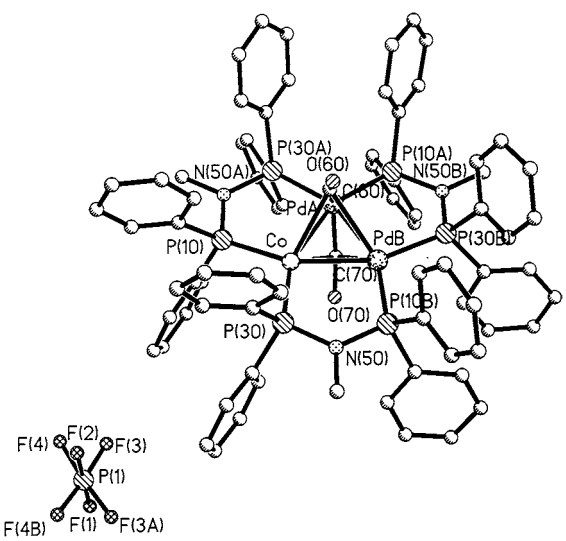

Fig. 1. View of the structure of the cation $[CoPd_2(\mu_3\text{-}CO)_2(\mu\text{-dppam})_3]^+$ in **2c**. The labelling of the metal atoms is only intended to guide the reader as these atoms are crystallographically equivalent by disorder.

Table 1
Selected bond lengths [Å] and angles [°] for $[CoPd_2(\mu\text{-dppam})_3(\mu_3\text{-}CO)_2]PF_6$ (**2c**)

Pd(A)–Co	2.533(1)
Pd(A)–Pd(B)	2.533(1)
Pd(B)–Co	2.533(1)
Pd(A)–C(60)	2.45(2)
Pd(A)–C(70)	2.49(3)
Pd–P(10)	2.237(2)
Pd–P(30)	2.238(2)
Pd(B)–C(70)	2.53(2)
Pd(B)–C(60)	2.52(2)
Co–C(60)	1.80(3)
Co–C(70)	1.83(2)
Co–P(10)	2.237(2)
Co–P(30)	2.238(2)
P(30)–N(50)	1.702(8)
N(50)–C(51)	1.476(11)
O(60)–C(60)	1.28(3)
O(70)–C(70)	1.22(2)
P(10)–Co–P(30)	109.01(8)
P(10)–Co–C(60)	103.1(6)
P(30)–Co–C(60)	126.7(6)
P(10)–Co–C(70)	102.9(6)
P(30)–Co–C(70)	128.4(6)
C(60)–Co–C(70)	81.8(7)
Pd(A)–Co–Pd(B)	60.0
P(30)–N(50)–P(10B)	121.0(4)
Co–C(60)–Pd(A)	61.2(6)
Co–C(70)–Pd(A)	60.6(5)

reactions were not successful with **1d**, they worked well in the case of **1a** and **1b**.

2.2. Molecular structure of $[CoPd_2(\mu_3\text{-}CO)_2(\mu\text{-}dppam)_3]PF_6$ (**2c**)

The structure suffers threefold disorder about the axis passing through the centre of the metal triangle (Fig. 1). Each metal position has the occupation factors of 0.67 for Pd and 0.33 for Co. Due to the average value of the occupation at each metal position caused by the disorder, only an average value for the bond distances is observed. Selected parameters are given in Table 1.

This results in the three transition metal atoms building a pseudo equilateral triangle with an average metal–metal distance of 2.533(1) Å. This value is in good agreement with the metal–metal distances found for $[CoPd_2(\mu_3\text{-}CO)_2(CO)_2(\mu\text{-dppm})_2]PF_6$ (Pd–Pd = 2.559(1), Pd–Co = 2.620(2) Å) ([6]a) and is shorter than the Pd–Pd bond of $[Pd_2Cl_2(\mu\text{-dppa})_2]$ (2.635(1) Å) [10]. The two face-bridging carbonyl groups are not symmetrically bonded to all three metal atoms and are disordered with respect to the threefold axis perpendicular to the metal plane. This causes three equivalent positions for the carbonyl C atoms and rather large displacement parameters for the corresponding O atom which sits on the axis. The unsymmetrically bonded carbonyl groups have a shorter bond to a Co and a Pd atom and a longer bond to the other Pd atom [Co–C(60): 1.80(3), Pd(A)–C(60): 2.45(3), Pd(B)–C(60): 2.52(2), Co–C(70): 1.83(2), Pd(A)–C(70): 2.49(2), Pd(B)–C(70): 2.53(2) Å]. These values are also in good agreement with those for related dppm clusters ([6]a). Every metal–metal bond is bridged by a dppam ligand. The P–N–P angle α of the dppam ligands is around 121°, which is larger than in several dinuclear palladium complexes containing the dppa ligand where values of 116–119° have been observed [10].

In the literature, bridging versus chelating behaviour of the diphosphine ligand dppa is still matter of discussion. Whereas Farrar et al. [10] expect the smaller amino group to increase the propensity of this ligand to bridge two metal centres when compared with dppm, Ellermann et al. [11] report the formation of very stable four-membered complexes of the square-planar cations $[M(dppa)_2]^{n+}$ for Rh^{I}, Ir^{I} ($n = 1$) and Pt^{II} ($n = 2$), respectively [11]. Puddephatt ([1]d) postulated a major influence of the substituents at phosphorus on the co-ordination modes of ligands of the type $(X_2P)_2NR$ (R = Me, Et, X = F, OMe, O^{i}Pr) with the nitrogen atom substituents having less influence. In the synthesis of $[Pd_2Cl_2(\mu\text{-dppa})_2]$ no formation of a chelated by-product has been observed. This indicates that there must be a significant influence of the nitrogen atom substituents in our reaction, which favours to a certain extent chelation in the case of alkyl substituted bisphosphinoamines. This could be explained by steric effects as discussed for different complexes containing the ligands dppm, dppa and dppam complexes [12].

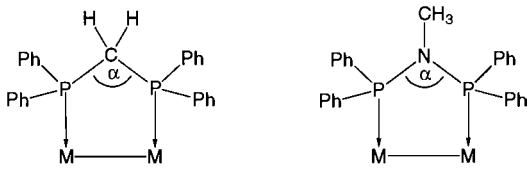

An important structural characteristic of co-ordinated diphosphines is the angle α. Numerous investigations reveal that in dppm or dppa complexes, the metal atoms and the co-ordinated diphosphines are (quasi) coplanar. However, in dppam complexes, the alkyl group on the nitrogen atom is sterically more demanding than the hydrogen atom in analogous dppa complexes. Interestingly, the five-membered ring in **2c** is almost planar (torsional angle Pd–P(30)–N(50)–P(10) = 1.53°) Bending of the methyl substituent at N(50) out of the plane (while retaining the M–P–N and P–N–P angles) would have resulted in a larger bite angle but also in an increased interaction between the methyl group and the P–Ph groups located at the ring face towards which the methyl group is bent. Steric factors could thus explain why formation of the dinuclear complex $[Pd_2Cl_2(\mu\text{-dppaSi})_2]$ is somewhat disfavoured compared with $[Pd_2Cl_2(\mu\text{-dppa})_2]$ whereas formation of $[PdCl_2(\mu\text{-dppaSi})]$, with a smaller angle α for the chelating dppaSi ligand, becomes more important [2].

2.3. Electrochemistry and coupled ESR measurements

The cyclic voltammetric behaviour of complexes $[CoPd_2(\mu_3\text{-}CO)_2(\mu\text{-dppm})_3]^+$ (**2a**), $[CoPd_2(\mu_3\text{-}CO)_2(\mu\text{-dppa})_3]^+$ (**2b**) and $[CoPd_2(\mu_3\text{-}CO)_2(\mu\text{-dppam})_3]^+$ (**2c**) is compared in Fig. 2 and exemplifies the redox propensity of the whole series of complexes studied here.

With reference to $[CoPd_2(\mu_3\text{-}CO)_2(\mu\text{-dppm})_3]^+$ (**2a**), controlled potential coulometry indicates that the anodic process involves a single-step two-electron oxidation whereas the first cathodic step involves a one-electron reduction, both redox changes being chemically reversible. Accordingly, in cyclic voltammetry at scan rates varying from 0.02 V s^{-1} to 1.00 V s^{-1}, both the oxidation and the first reduction exhibit an i_p(backward)/i_p(forward) ratio constantly equal to 1. However, it must be pointed out that the peak-to-peak separation of 109 mV exhibited by the anodic process even at the lowest scan rate of 0.02

$V\,s^{-1}$ significantly departs from the value of 42.2 mV theoretically expected for two reversible one-electron transfers occurring at the same potential value [13]. This indicates an electrochemically quasi-reversible process suggesting that significant structural changes follow the two-electron removal. In contrast, the one-electron addition processes possess features of electrochemical reversibility, thus indicating retention of the original structure [3,4]. A second cathodic step having features of chemical reversibility is present at notably negative potential values. Because it is close to solvent discharge, we could not perform macroelectrolysis tests. However, based on its peak-height, we confidently assume that it involves a one-electron transfer.

Substitution of the CH_2 unit for the NR (R = H, Me) group in the backbone of the diphosphine ligands causes destabilization of all the redox couples. In particular, whereas for $[CoPd_2(\mu_3\text{-}CO)_2(\mu\text{-}dppam)_3]$ (**2c**) only the two-electron oxidation becomes complicated by relatively slow chemical reactions, all the redox changes for $[CoPd_2(\mu_3\text{-}CO)_2(\mu\text{-}dppa)_3]^+$ (**2b**) are accompanied by fast degradation.

In agreement with the changes observed when the dppm ligand is replaced by dppa and dppam, the mixed–ligand complexes $[CoPd_2(\mu_3\text{-}CO)_2(\mu\text{-}dppm)_2(\mu\text{-}dppa)]$ (**3b**), $[CoPd_2(\mu_3\text{-}CO)_2(\mu\text{-}dppm)_2(\mu\text{-}dppam)]$ (**3c**), $[CoPd_2(\mu_3\text{-}CO)_2(\mu\text{-}dppm)_2(\mu\text{-}dppaSi)]^+$ (**3d**) and $[CoPd_2(\mu_3\text{-}CO)_2(\mu\text{-}dppm)(\mu\text{-}dppa)_2]$ (**4a**) also exhibit re dox changes which do not always afford stable

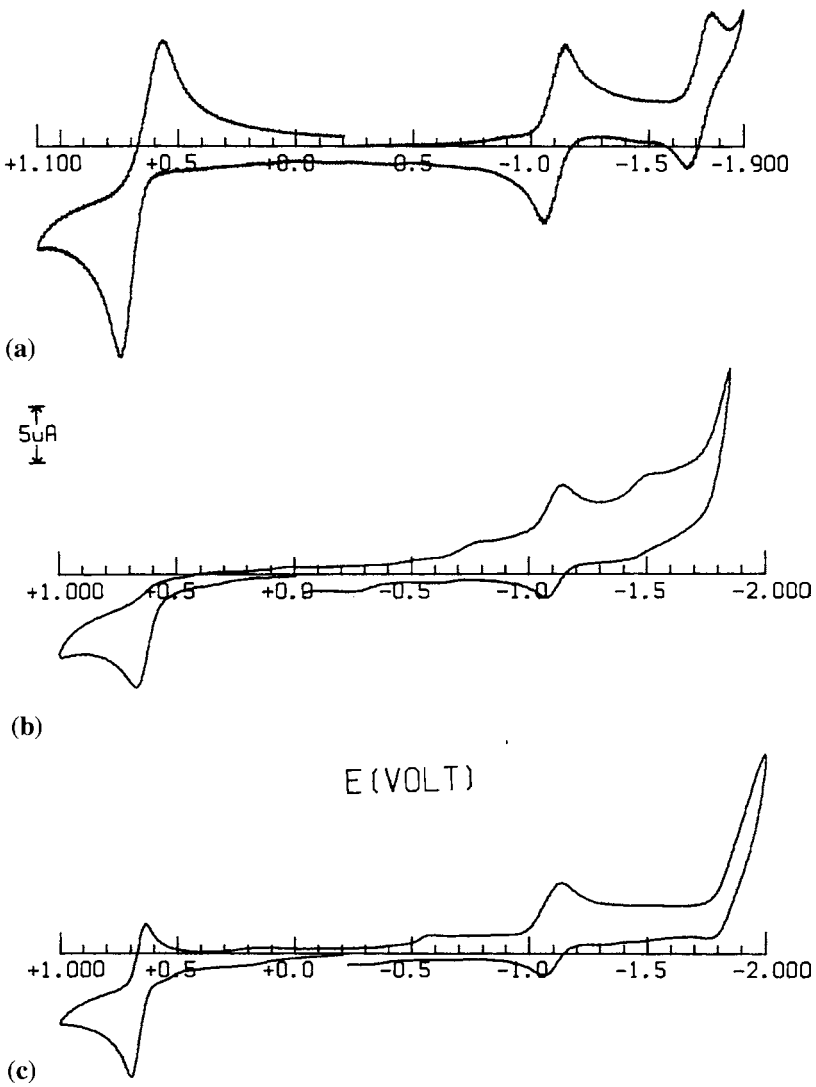

Fig. 2. Cyclic voltammetric responses recorded at a platinum electrode on a THF solution containing $[Bu_4N]PF_6$ (0.2 mol dm^{-3}) and: (a) $[CoPd_2(\mu_3\text{-}CO)_2(\mu\text{-}dppm)_3]^+$ (**2a**) (8×10^{-4} mol dm^{-3}); (b) $[CoPd_2(\mu_3\text{-}CO)_2(\mu\text{-}dppa)_3]^+$ (**2b**) (6×10^{-4} mol dm^{-3}); (c) $[CoPd_2(\mu_3\text{-}CO)_2(\mu\text{-}dppam)_3]^+$ (**2c**) (6×10^{-4} mol dm^{-3}). Scan rate 0.02 $V\,s^{-1}$.

Table 2
Formal electrode potentials (in V, versus SCE) and peak-to-peak separation (in mV) for the redox changes exhibited by the $CoPd_2$ clusters

Complex	$E^{\circ\prime}_{3+/+}$	ΔE_p^a	$E^{\circ\prime}_{+/0}$	ΔE_p^b	$E^{\circ\prime}_{0/-}$	ΔE_p^b	Solvent
$[CoPd_2(\mu_3\text{-}CO)_2(\mu\text{-}dppm)_3]^+$ (**2a**)	+0.65	109	−1.11	73	−1.71	75	THF
	+0.55	136	−1.32	76	−1.86	95	CH_2Cl_2
$[CoPd_2(\mu_3\text{-}CO)_2(\mu\text{-}dppa)_3]^+$ (**2b**)	+0.64[c]		−1.10[d]	82	e		THF
	+0.60[c]		−1.22[d]	90	e		CH_2Cl_2
$[CoPd_2(\mu_3\text{-}CO)_2(\mu\text{-}dppam)_3]^+$ (**2c**)	+0.70[d]	48	−1.08[d]	76	e		THF
	+0.54[d]	44	−1.36		e		CH_2Cl_2
$[CoPd_2(\mu_3\text{-}CO)_2(\mu\text{-}dppm)_2(\mu\text{-}dppa)]^+$ (**3b**)	+0.66[d]	113	−1.10	98	−1.75[b]	70	THF
	+0.55[d]	108	−1.28[c]	74	e		CH_2C1_2
$[CoPd_2(\mu_3\text{-}CO)_2(\mu\text{-}dppm)(\mu\text{-}dppa)_2]^+$ (**4a**)	+0.65[d]	106	−1.12	80	e		THF
	+0.61[c]		−1.30[d]	78	e		CH_2C1_2
$[CoPd_2(\mu_3\text{-}CO)_2(\mu\text{-}dppm)_2(\mu\text{-}dppam)]^+$ (**3c**)	+0.63[c]		−1.10[d]	72	e		THF
	+0.42[c]		−1.32[d]	74	e		CH_2Cl_2
$[CoPd_2(\mu_3\text{-}CO)_2(\mu\text{-}dppm)_2(\mu\text{-}dppaSi)]^+$ (**3d**)	+0.68[d]	88	−1.13[d]	98	e		THF
	+0.56[d]	132	−1.35[c]		e		CH_2Cl_2
$[CoPd_2(\mu_3\text{-}CO)_2(\mu\text{-}dppm)_2(CO)_2]^+$			−0.64[d]	170	−1.07[d]	134	THF
			−0.87[c]		−1.35[c]		CH_2Cl_2
			−0.77[d,f]		−1.00[d,f]		DMSO

[a] Measured at 0.02 V s^{-1}.
[b] Measured at 0.2 V s^{-1}.
[c] Peak-potential value for irreversible processes.
[d] Complicated by slow chemical reactions.
[e] Difficult to measure because of the solvent discharge.
[f] From [5].

products. The electrochemical parameters for all the complexes studied are compiled in Table 2.

It is interesting that the monocation $[CoPd_2(\mu_3\text{-}CO)_2(\mu\text{-}dppm)_2(CO)_2]^+$ which contains a terminal CO ligand bound to palladium only undergoes two separated one-electron reductions, which are followed by chemical complications. It is hence evident that incorporation of the third bidentate dppm ligand in the $CoPd_2(\mu_3\text{-}CO)_2$ assembly significantly modifies the HOMO/LUMO frontier orbitals, allowing access to their oxidized congeners.

We note that for the somewhat related homonuclear complexes $[Cu_3(\mu_3\text{-}C{\equiv}CR)_2(\mu\text{-diphosphine})_3]^+$, a quasi-reversible Cu(I)/Cu(II) oxidation was observed. The ease of oxidation was in line with the electron donating character of the bridging diphosphine but the stability of the oxidized products appeared unaffected by the nature of the diphosphine [14].

Fig. 3 shows the X-band ESR spectra of the electrogenerated neutral species $[CoPd_2(\mu_3\text{-}CO)_2(\mu\text{-}dppm)_3]$ in THF solution, together with the corresponding simulated spectra [15].

The line-shape analysis of the signal recorded at 100 K, Fig. 3(a), is suitably carried out in terms of the $S = 1/2$ electron spin Hamiltonian and provides evidence for the strong metal character of the signal ($g_{aniso} > g_e = 2.0023$; $\Delta H_{aniso} > 15$ G; $a_{aniso}(Co, Pd) < \Delta H_{aniso}$). The broad and unresolved anisotropic axial spectrum is indicative of the presence of significant overall orbital contribution within the bimetallic core, which likely obscures the hyperfine metal splitting as well as the less intense (if any) superhyperfine couplings of the unpaired electron with the ligand system ($I(^{31}P) = 1/2$, $I(^1H) = 1/2$). On the other hand, the absence of both hpf and shpf splittings is not surprising in view of the low local symmetry of the $CoPd_2$ assembly (C_{2v}), which causes effective shortening of the electron spin relaxation times and hence an overall line broadening. When rising the temperature at the glassy-fluid transition ($T = 166$ K), the anisotropic signal drops out and a broad isotropic signal appears, the parameters of which correspond well to the glassy ones. This confirms that the overall cluster geometry is retained under different experimental conditions. The absence of the Co ($I(^{59}Co) = 7/2$) and Pd ($I(^{105}Pd) = 5/2$) hyperfine resolution as well as that of the corresponding phosphorous superhyperfine one is a consequence of the actual isotropic line-width, which allows an upper limit for the relevant magnetic interactions to be assigned: $\Delta H_{iso}(200\ K) = 65\ G \geq a_{iso}(200\ K)(Co, {}^{105}Pd) \geq a_{iso}(200\ K)$ (P); $\Delta H_{iso}(200\ K)/7 \geq a_{iso}(200\ K)(Co)$; $\Delta H_{iso}(200\ K)/10 \geq a_{iso}(200\ K)({}^{105}Pd)$.

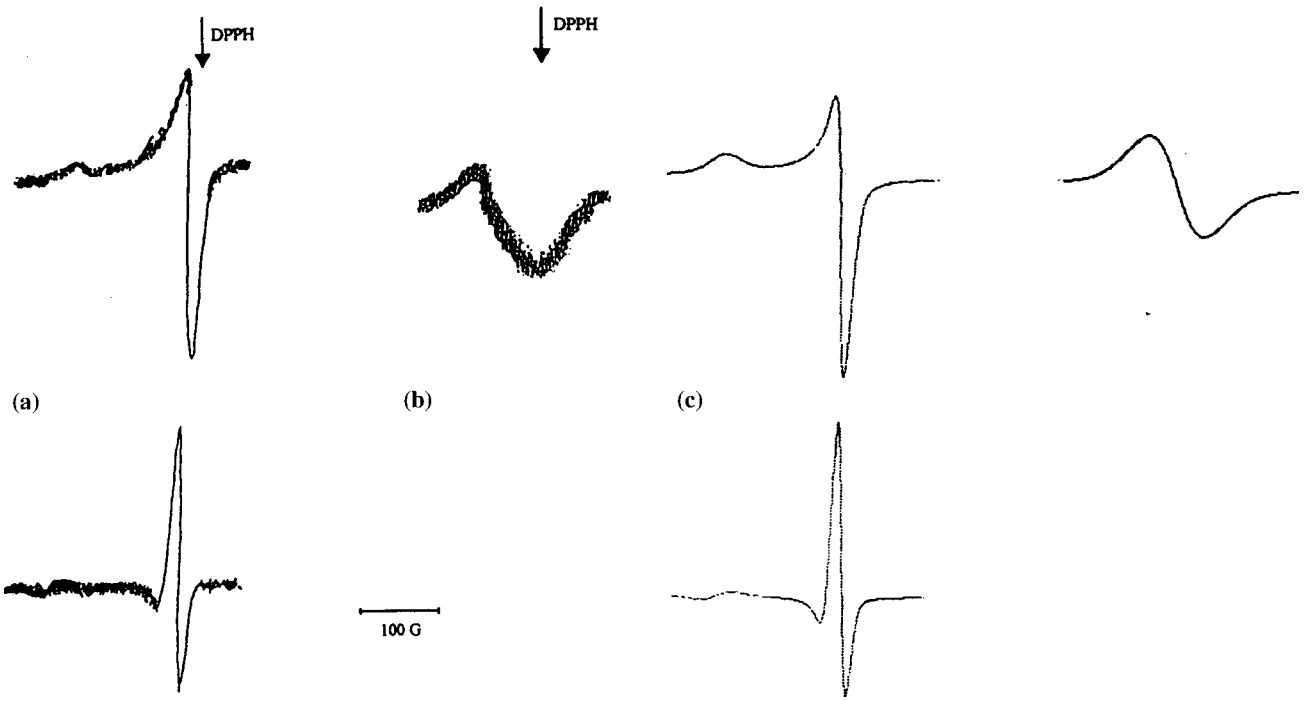

Fig. 3. X-band EPR spectra of the electrogenerated species $[CoPd_2(\mu_3\text{-}CO)_2(\mu\text{-}dppm)_3]^{\bullet}$. in THF solution. (a) $T = 100$ K, first and second derivative mode; (b) $T = 200$ K; (c) corresponding simulated spectra.

When the paramagnetic sample was frozen again, the features for the glassy sample were quantitatively restored. Frozen solutions from electroreduction of $[CoPd_2(\mu_3\text{-}CO)_2(\mu\text{-}dppam)_3]^+$ (**2c**) display ESR features quite similar to those of $[CoPd_2(\mu_3\text{-}CO)_2(\mu\text{-}dppm)_3]^+$ (**2a**), indicating that the change of ligand does not affect the paramagnetic parameters, likely because the fundamental geometry is maintained. Nevertheless, at the glassy-fluid transition, the axial signal tends to drop out as a consequence of the above outlined chemical complications. As a matter of fact, upon refreezing, the original signal is no more recovered.

A quite different paramagnetic behaviour is obtained upon electroreduction of $[CoPd_2(\mu_3\text{-}CO)_2(\mu\text{-}dppa)_3]^+$ (**2b**). As shown in Fig. 4, the broad, well structured rhombic spectrum obtained at liquid nitrogen temperature displays g_i values characteristic of a species with a paramagnetic metal character and large anisotropic hpf splittings.

The best fit parameters are indicative of a $S = 1/2$ cobalt paramagnetic radical ($g_i \neq g_e$), without any direct evidence for ^{105}Pd and/or phosphorus splittings.

In agreement with the electrochemical data, the glassy spectrum suggests that the instantaneously electrogenerated radical $[CoPd_2(\mu_3\text{-}CO)_2(\mu\text{-}dppa)_3]^{\bullet}$ is unstable and undergoes fast fragmentation to a long-lived paramagnetic cobalt species. In fluid solution, the spectrum evolves to a new broad and unresolved signal displaying quite different g_{iso} value, which slowly and irreversibly drops out.

Table 3 summarizes the temperature-dependent X-band ESR parameters of the spectra obtained upon exhaustive one-electron reduction of the monocations $[CoPd_2(\mu_3\text{-}CO)_2(dppm)_3]^+$ (**2a**), $[CoPd_2(\mu_3\text{-}CO)_2(\mu\text{-}dppa)_3]^+$ (**2b**) and $[CoPd_2(\mu_3\text{-}CO)_2(\mu\text{-}dppam)_3]^+$ (**2c**).

In conclusion, the paramagnetic behaviour recorded upon electroreduction of $[CoPd_2(\mu_3\text{-}CO)_2(\mu\text{-}dppm)_3]^+$ (**2a**), $[CoPd_2(\mu_3\text{-}CO)_2(\mu\text{-}dppa)_3]^+$ (**2b**) and $[CoPd_2(\mu_3CO)_2(\mu\text{-}dppam)_3]^+$ (**2c**) indicates that the generated $S = 1/2$ unpaired electron is basically located in a metal-centred SOMO. In the case of **2a** and **2c** the

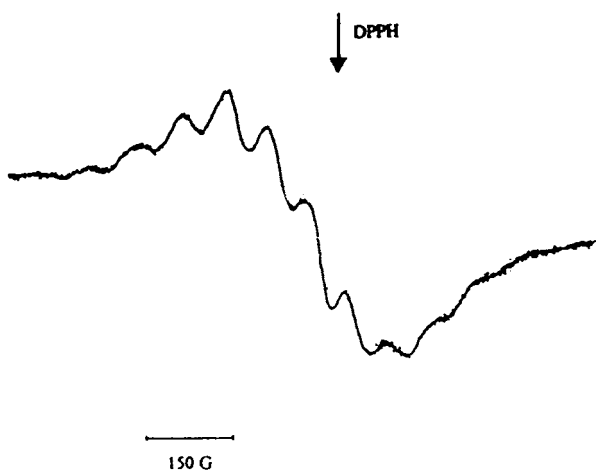

Fig. 4. X-band EPR spectrum of the species arising from electroreduction of $[CoPd_2(\mu_3\text{-}CO)_2(\mu\text{-}dppa)_3]^+$ (**2b**) in THF at $T = 100$ K.

Table 3
Temperature-dependent X-band EPR parameters for the paramagnetic species obtained upon electroreduction of $[CoPd_2(\mu_3\text{-}CO)_2(\mu\text{-}dppm)_3]^+$ (**2a**), $[CoPd_2(\mu_3\text{-}CO)_2(\mu\text{-}dppa)_3]^+$ (**2b**) and $[CoPd_2(\mu_3\text{-}CO)_2(\mu\text{-}dppam)_3]^+$ (**2c**) in THF solution (a_i in Gauss; $g_i = \pm 0.008$; $a_i = \pm 8$ G)

Complex	$g_{\|\|}$	$g_\perp$	$\langle g \rangle^{a,b}$	g_{iso}	$a_{\|\|}$	$a_\perp$	$\langle a \rangle^{c,d}$	a_{iso}
2a	2.095	2.009	2.038	2.038	<34	<15	<21	< 65
2b	2.192[b]	2.142[b]	2.095	2.192	70	67	69	<100
		1.950[b]				70		
2c	2.093	2.006	2.035	—	<32	<14	<20	

[a] $\langle g \rangle = 1/3(g_{\|\|}+2g_\perp)$ for axial symmetry.
[b] $\langle g \rangle = 1/3(g_l+g_m+g_h)$ for rhombic symmetry.
[c] $\langle a \rangle = 1/3(a_{\|\|}+2a_\perp)$ for axial symmetry.
[d] $\langle a \rangle = 1/3(a_l+a_m+a_h)$ for rhombic symmetry.

unpaired electron is largely localized onto the triangular metallic skeleton. In the case of **2b**, the frontier orbitals assume a strong antibonding character.

3. Experimental section

3.1. Reagents and techniques

All reactions were performed in Schlenk-type flasks under nitrogen. Solvents were dried and distilled under nitrogen: tetrahydrofuran and diethylether over sodium benzophenone ketyl; *n*-pentane over sodium and dichloromethane and acetonitrile over P_2O_5. Water was degassed and saturated with nitrogen. Nitrogen (Air Liquide R-grade) was passed through BASF R3-11 catalyst and molecular sieve columns to remove residual oxygen and water. Unless otherwise stated, reagents were obtained from commercial sources and used without further purification. Elemental analyses were performed by the Service Central de Microanalyses du CNRS. Infrared spectra were recorded in the 4000–400 cm^{-1} region on a Bruker IFS 66 spectrometer. The ^1H and $^{31}P\{^1H\}$ spectra were recorded at 200.13 and 81.02 MHz, respectively, on a Bruker AC 300 instrument. Proton chemical shifts are positive downfield relative to external $SiMe_4$. $^{31}P\{^1H\}$-NMR spectra were externally referenced to 85% H_3PO_4 in H_2O, with downfield chemical shifts reported as positive. Due to the different non-equivalent phosphorus atoms of the Pd–Co clusters their chemical shifts are attributed referring to the following scheme for the tri- and tetranuclear compounds:

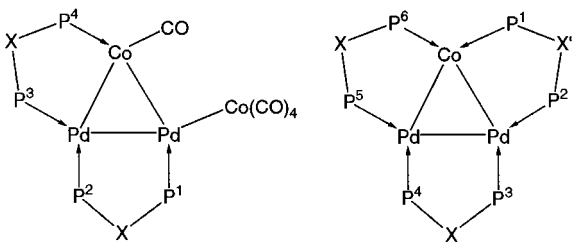

for clusters with mixed-ligand sets

Materials and apparatus for the electrochemical and EPR measurements have been described elsewhere [16]. Potential values are referenced to the saturated calomel electrode (SCE) and are given with a typical accuracy of ± 5 mV. Under our experimental conditions the one-electron oxidation of ferrocene occurs at $+0.38$ V in CH_2Cl_2 ($\Delta E_p = 82$ mV at 0.2 V s^{-1}) and at $+0.53$ V in THF ($\Delta E_p = 86$ mV at 0.2 V s^{-1}).

3.2. Synthesis

The ligands dppa [7] and dppaSi [2] and the complex $[Pd_2Cl_2(\mu\text{-}dppa)_2]$ [7] were prepared according to literature methods. Solutions of $Na[Co(CO)_4]$ were prepared by Na/Hg reduction of THF solutions of $[Co_2(CO)_8]$.

3.2.1. $[Co_2Pd_2(\mu_3\text{-}CO)_2(CO)_5(\mu\text{-}dppa)_2]$ (**1b**)

A filtered solution of $Na[Co(CO)_4]$ in THF (2.14 mmol, 9.1 ml) was added to a cooled (-78°C) and stirred suspension of $[Pd_2Cl_2(\mu\text{-}dppa)_2]$ (1.13 g, 1.07 mmol) in THF (75 ml). The reaction temperature was progressively raised to 0°C. The colour of the mixture slowly turned from orange to deep violet. The temperature was then raised to 20°C and the colour changed to deep green. After stirring for 5 h the mixture was filtered, the volume of the solvent reduced to 20 ml and *n*-pentane added to precipitate a deep green powder of **1b**, which was washed with water, to remove residual ionic species, Et_2O and *n*-pentane and dried. The product was recrystallized from CH_2Cl_2/*n*-pentane to afford pure **1b** in 86% yield. Anal. Calcd. for $C_{55}H_{42}Co_2N_2O_7P_4Pd_2$: C, 50.91; H, 3.26; N, 2.16%. Found: C, 49.91; H, 3.57; N, 2.15%. IR (KBr): ν(CO) 2010 (vs), 1986 (s), 1928 (sh), 1907 (vs) cm^{-1}. IR (THF): ν(CO) 2015 (vs), 1992 (ms), 1933 (s), 1920 (m, ski) cm^{-1}. ^1H-NMR (acetone-d_6): δ 7.79–7.20 (40 H, m, phenyl-H), 6.59 (s, 1H, NH), 6.54 (s, 1H, NH). The nitrogen protons exchange with D_2O. $^{31}P\{^1H\}$-NMR (acetone-d_6): δ 77.1 (dm, 1P, $J(P^1\text{–}P^4) = 166$ Hz, $P^4 \rightarrow$ Co), 51.7 (ddd, 1P, $J(P^1\text{–}P^4) = 166$ Hz, $P^1 \rightarrow P^2) = 154$ Hz, $P^1 \rightarrow$ Pd), 48.1 (dd, 1P, $J(P^2\text{–}P^3) = 54$ Hz, $P^3 \rightarrow$ Pd),

42.4 (ddd, 1P, $J(P^2-P^3) = 54$ Hz, $J(P^2-P^4) = 24$ Hz, $P^2 \rightarrow Pd$). Mass spectrum (FAB^+): m/z 1126.9 (M^+-$Co(CO)_4$).

3.2.2. $[CoPd_2(\mu_3\text{-}CO)_2(\mu\text{-}dppa)_3][PF_6]$ (2b)

Dppa (0.354 g, 0.920 mmol) and $[NH_4][PF_6]$ (0.195 g, 1.20 mmol) were added to a solution of **1b** (1.17 g, 0.900 mmol) in THF (30 ml). Immediately after addition of the diphosphine, the reaction mixture turned from green to red, and after the solution has been stirred for 15 min at room temperature, its colour had turned to yellow–brown. Stirring was continued for 4 h. The solvent was removed in vacuo, and the residue was washed with water and dried. Purification was achieved by dissolving the compound in THF, filtering the solution, and precipitating the brown solid with a mixture of Et_2O/*n*-hexane. The resulting product was recrystallized from CH_2Cl_2/*n*-hexane, affording brown needles of **2b** (92%). Anal. Calcd. for $C_{74}H_{63}CoF_6N_3O_2P_7Pd_2$: C, 54.57; H, 3.90; N, 2.58%. Found: C, 54.95; H, 3.94; N, 2.41%. IR (KBr): ν(CO) 1868 (vs) cm^{-1}. ^{1}H-NMR (C_3D_6O), δ 7.30–7.17 (60H, m, phenyl-H), 6.93 (1H, br-s, NH), 6.38 (2H, br-s, N<u>H</u>). The nitrogen protons exchange with D_2O). $^{31}P\{^1H\}$-NMR (C_3D_6O), δ 75.9 (m, 2P, $P \rightarrow Co$), 41.6 (dm, 2P, $P \rightarrow Pd$), 40.0 (m, 2P, $P \rightarrow Pd$). Mass spectrum (FAB^+): m/z 1484.0 (M^+-PF_6).

3.2.3. $[CoPd_2(\mu_3\text{-}CO)_2(\mu\text{-}dppam)_3][PF_6]$ (2c)

Excess DBU (0.912 g, 6.00 mmol) was added to a solution of **2b** (1.63 g, 1.00 mmol) in THF (20 ml) at room temperature. After stirring for 30 min, an excess of methyliodide (0.852 g, 6.00 mmol) was added and stirring was continued for 2 h. The mixture was filtered and the volume of the solvent was reduced in vacuo. A yellow brown solid was precipitated on addition of excess *n*-pentane. Recrystallization from CH_2Cl_2/*n*-pentane afforded **2c** in 71% yield. Anal. Calcd. for $C_{77}H_{69}CoF_6N_3O_2P_7Pd_2$: C, 55.35; H, 4.16; N, 2.51%. Found: C, 52.39; H, 4.38; N, 2.04%. IR (KBr): ν(CO) 1856 (vs) cm^{-1}. ^{1}H-NMR (C_3D_6O), δ 7.36–7.10 (60H, m, phenyl-H), 2.24 (br-s, 3H, NCH_3), 1.98 (br-s, 6H, NCH_3). $^{31}P\{^1H\}$-NMR (C_3D_6O): δ 100.1 (m, 2P, $P \rightarrow$ Co), 67.3 (dm, 2P, $P \rightarrow Pd$), 63 8 (m, 2P, $P \rightarrow Pd$).

3.2.4. $[CoPd_2(\mu_3\text{-}CO)_2(\mu\text{-}dppm)_2(\mu\text{-}dppa)][PF_6]$ (3b)

Dppa (0.536 g, 1.39 mmol) and $[NH_4][PF_6]$ (0.238 g, 1.46 mmol) were added to a solution of $[Co_2Pd_2(\mu_3\text{-}CO)_2(CO)_5(\mu\text{-}dppm)_2]$ (**1a**) (1.74 g, 1.34 mmol) in THF (30 ml). Immediately after addition of the diphosphine, the reaction mixture turned from green to red, and after 15 min of stirring at room temperature, its colour had turned to yellow–brown. Stirring was continued for 4 h. The solution was filtered and the solvent was removed in vacuo. The residue was washed with water and dried. Purification was achieved by dissolving the compound in THF, filtering the solution, and precipitating the brown solid with a mixture of Et_2O/*n*-hexane. The resulting product was recrystallized from CH_2Cl_2/*n*-hexane, affording brown needles of **3b** (88%). Anal. Calcd. for $C_{76}H_{65}CoF_6NO_2P_7Pd_2$: C, 56.11; H, 4.03; N, 0.86%. Found: C, 55.70; H, 4.36; N, 1.08. IR(THF): $\nu(CO) = 1854$ cm^{-1}. ^{1}H-NMR (acetone-d_6): δ 7.30–6.98 (m, 60H, phenyl-H), 6.13 (br-s, 1 H, NH), 5.00 (sept, 2H, CH_2), 4.42 (t, 2H, CH_2). $^{31}P\{^1H\}$-NMR (acetone-d_6): δ 74.2 (m, 1P, $P^1 \rightarrow Co$), 37.0 (dm, 1P, $P^2 \rightarrow Pd$), 26.0 (m, 1P, $P^6 \rightarrow Co$), -8.27 (m, 3P, $P^{3,4,5} \rightarrow$ Pd).

3.2.5. $[CoPd_2(\mu_3\text{-}CO)_2(\mu\text{-}dppm)_2(\mu\text{-}dppam)][PF_6]$ (3c)

To a solution of 0.159 g (0.098 mmol) of $[CoPd_2(CO)7(\mu\text{-}dppm)_2(\mu\text{-}dppa)][PF_6]$ in 10 ml THF was added excess DBU (0.03 ml, 0.075 g, 0.49 mmol) and excess methyl iodide (0.139 g, 0.98 mmol). Gas evolution was observed and stirring was continued for 30 min. Then the solution was filtered and its volume was reduced to 10 ml. Addition of *n*-hexane precipitated a brown powder. The product was recrystallized twice from CH_2Cl_2/*n*-hexane to afford a brown microcrystalline solid of pure **3c** in 87% yield. Anal. Calcd. for $C_{77}H_{67}CoF_6NO_2P_7Pd_2$: C, 56.36; H, 4.12; N, 0.85%. Found: C, 55.64; H, 4.25; N, 1.14%. IR (THF): $\nu(CO) = 1853$ cm^{-1}. ^{1}H-NMR (acetone-d_6): δ 7.38–6.95 (m, 60H, phenyl-H), 4.98 (m, 2H, CH_2), 4.32 (m, 2H, CH_2), 1.98 (s, 3H, NCH_3). $^{31}P\{^1H\}$-NMR (acetone-d_6): δ 100.2 (m, 1P, $P^1 \rightarrow Co$), 62.4 (dm, 1P, $P^2 \rightarrow$ Pd), 26.1 (m, 1P, $P^6 \rightarrow Co$), -7.0 (m, 3P, $P^{3,4,5} \rightarrow Pd$).

3.2.6. $[CoPd_2(\mu_3\text{-}CO)_2(\mu\text{-}dppm)_2(\mu\text{-}dppaSi)][PF_6]$ (3d)

This cluster was prepared following the procedure described for **3b**.

Data for **3d**: $[Co_2Pd_2(\mu_3\text{-}CO)_2(CO)_5(\mu\text{-}dppm)_2]$ (**1a**) (0.190 g, 0.147 mmol) in 30 ml THF, dppaSi (0.087 g, 0.147 mmol), $[NH_4][PF_6]$ (0.026 g, 0.161 mmol). Cluster **3d** was obtained as a brown microcrystalline powder. Yield: 81%. Anal Calcd. for $C_{85}H_{85}CoF_6NO_5P_7Pd_2Si$: C, 55.75; H, 4.68; N, 0.76%. Found: C, 54.95; H, 4.32; N, 0.66%. IR (THF): $\nu(CO) = 1854$ cm^{-1}. ^{1}H-NMR (acetone-d_6): δ 7.49–6.96 (m, 60H, phenyl-H), 4.99 (m, 2H, CH_2), 4.37 (m, 2H, CH_2), 3.35 (q, 6H, $OC\underline{H}_2CH_3$), 2.39 (m, 2H, NCH_2), 0.89 (t, 9H, $OCH_2C\underline{H}_3$), 0.34 (m, 2H, $CH_2C\underline{H}_2CH_2$), -0.40 (m, 2H, CH_2Si). $^{31}P\{^1H\}$-NMR (acetone-d_6): δ 101.9 (m, 1P, $P^1 \rightarrow Co$), 62.3 (dm, 1P, $P^2 \rightarrow Pd$), 26.2 (m, 1P, $P^6 \rightarrow Co$), -7.2 (m, 3P, $P^{3,4,5} \rightarrow Pd$).

3.2.7. $[CoPd_2(\mu_3\text{-}CO)_2(\mu\text{-}dppm)(\mu\text{-}dppa)_2][PF_6]$ (4a) and $[CoPd_2(\mu_3\text{-}CO)_2(\mu\text{-}dppaSi)(dppa)_2][PF_6]$ (4d)

These clusters were prepared following the procedure described for **2b**.

Data for **4a**: $[Co_2Pd_2(\mu_3\text{-}CO)_2(CO)_5(\mu\text{-}dppa)_2]$ (**1b**) (0.202 g, 0.156 mmol) in 30 ml THF, dppm (0.064 g,

0.166 mmol), $[NH_4][PF_6]$ (0.028 g, 0.172 mmol). Cluster **4a** was obtained as a yellow brown microcrystalline powder in 79% yield. Anal. Calcd. for $C_{75}H_{64}CoF_6N_2O_2P_7Pd_2$: C, 55.34; H, 3.96; N, 1.72%. Found: C, 55.20; H, 4.36; N, 1.48%. IR (THF): $\nu(CO) = 1860$ cm^{-1}. ^{1}H-NMR (acetone-d_6): 7.67–6.98 (m, 60H, phenyl-H), 6.85 (br-s, 1H, NH), 6.20 (br-s, 1H, NH), 4.48 (t, 2H, CH_2). $^{31}P\{^1H\}$-NMR (acetone-d_6): 79.4 (m, 1P, $P^6 \rightarrow Co$), 43.3 (m, 3P, $P^{3,4,5} \rightarrow Pd$), 26.6 (m, 1P, $P^1 \rightarrow Co$), −7.5 (m, 1P, $P^2 \rightarrow Pd$).

Data for ***4d***: $[Co_2Pd_2(\mu_3\text{-}CO)_2(CO)_5(\mu\text{-dppa})_2]$ (**1b**) (0.060 g, 0.046 mmol) in 10 ml THF, dppaSi (0.029 g, 0.049 mmol), $[NH_4][PF_6]$ (0.0085 g, 0.052 mmol). Cluster **4d** was obtained as a brown microcrystalline powder in 88% yield. Anal. Calcd. for $C_{83}H_{83}CoF_6N_3O_5P_7Pd_2Si$: C, 54.38; H, 4.56; N, 2.29%. Found: C, 54.85; H, 4.36; N, 1.50%. IR (THF): $\nu(CO) = 1863$ cm^{-1}. ^{1}H-NMR (acetone-d_6): 7.69–6.95 (m, 60H, phenyl-H), 6.71 (brs, 1H, NH), 6.24 (br-s, 1H, NH), 3.37 (q, 2H, OCH_2), 2.48 (m, 2H, NCH_2), 0.97 (s, 9 H, $OCH_2C\underline{H}_3$), 0.42 (m, 2H, $CH_2\underline{CH}_2CH_2$), −0.35 (m, 2H, CH_2Si). $^{31}P\{^1H\}$-NMR (acetone-d_6): 101.4 (m, 1P, $P^6 \rightarrow Co$), 79.5 (m, 1P, $P^1 \rightarrow Co$), 63.5 (m, 1P, $P^5 \rightarrow Pd$), 45.4 (m, 3P, $P^{2,3,4} \rightarrow Pd$).

Table 4
Crystal data and structure refinement for $[CoPd_2(\mu_3\text{-}CO)_2(\mu\text{-dppam})_3]PF_6$ (**2c**)

Empirical formula	$C_{77}H_{69}CoF_6N_3O_2P_7Pd_2$
Formula weight	1670.88
Crystal system	Trigonal
Space group	$P\bar{3}$
Unit cell dimensions	
a (Å)	15.5079(6)
b (Å)	15.5079(6)
c (Å)	11.6143(6)
α (°)	90
β (°)	90
γ (°)	120
Volume	2419.0(2) Å^3
Z	3
Density (calculated)	1.147 g cm^{-3}
Absorption coefficient	0.701 mm^{-1}
$F(000)$	846
Crystal size	$0.16 \times 0.08 \times 0.07$ mm
θ range for data collection	1.52–25.00°
Limiting indices	$-22 < h < 17$ $-19 < k < 22$ $-16 < l < 15$
Reflections collected	14097
Independent reflections	5640 [R(int) = 0.0595]
Data/restraints/parameters	5506/1/314
Goodness-of-fit on F^2	1.116
R ($I > 2\sigma(I)$)	0.0619
Rw	0.1487
Absolute structure parameter	0.02(4)
Extinction coefficient	0.0035(7)
Weighting scheme	$w = 1/[\sigma^2(F_o^2) + (0.0917P)^2 + 0.82P)]$ $P = (F_o^2 + 2F_c^2)/3$
Largest difference peak and hole	1.737 and −0.501 e Å^{-3}

3.3. X-ray structure determination of $[CoPd_2(\mu\text{-dppa})_3(\mu_3\text{-}CO)_2]PF_6$ (2b)

Crystal data and experimental details are given in Table 4. The X-ray data were collected at room temperature on a Siemens SMART CCD area detector diffractometer using graphite monochromated Mo–K_α radiation ($\lambda = 71.073$ pm), a nominal crystal-to-detector distance of 3.85 cm and 0.3° ω-scan frames. Corrections for Lorentz polarization effects and an empirical absorption correction with the program SADABS were applied [17]. The structures were solved by direct methods (SHELXS86). Refinement was performed by the full-matrix least-squares method based on F^2 (SHELXL93). All non-hydrogen atoms were refined anisotropically and the hydrogen atoms were included in idealized positions. The structure is threefold disordered with respect to the centre of the metal triangle. Each metal position has the occupancy factors of 0.67 for Pd and 0.33 for Co. The two face-bridging carbonyl groups are not symmetrically bonded to all three metal atoms which causes three equivalent positions for the carbonyl C atoms and rather large displacement parameters for the corresponding O atom. The PF_6^- anion is strongly disordered and was solved with a model of six F atoms in the equatorial plane.

Selected bond distances and angles are given in Table 1. Atomic co-ordinates, thermal parameters and a complete list of bond distances and angles have been deposited at the Cambridge Crystallographic Data Centre.

Acknowledgements

We are grateful to the Centre National de la Recherche Scientifique (Paris), the Commission of the European Communities (contract CHRX-CT93-0277) and the Ministère des Affaires Etrangères (Paris) (Amadeus Programme) for financial support and to the ERASMUS programme (ICP-95-UK-3125/13, Dr A.K. Smith) and the Liverpool University (Dr S.J. Higgins) for allowing M.K. Mc C. to work in the Strasbourg Laboratory. P.Z. gratefully acknowledges the financial support of CNR (Rome) and is also indebted to Mrs Giuseppina Montomoli for technical assistance.

References

[1] (a) J.T. Mague, J. Cluster Sci. 6 (1995) 217. (b) P. Bhattacharyya, J.D. Woollins, Polyhedron 14 (1995) 3367. (c) M.S.

Balakrishna, Y. Sreenivasa Reddy, S.S. Krishnamurthy, J.F. Nixon, J.C.T.R. Burckett St. Laurent, Coord. Chem. Rev. 129 (1994) 1. (d) R.J. Puddephatt, Chem. Soc. Rev. 12 (1983) 99 and references cited therein. (e) M. Knorr, E. Hallauer, V. Huch, M. Veith, P. Braunstein, Organometallics 15 (1996) 3868. (f) M. Knorr, P. Braunstein, A. Tiripicchio, F. Ugozzoli, J. Organomet. Chem. 526 (1996) 105.

[2] I. Bachert, P. Braunstein, R. Hasselbring, New. J. Chem. 20 (1996) 993.

[3] P. Zanello, Struct. Bonding 79 (1992) 101–214.

[4] P. Zanello, In: P. Zanello (Ed.), Stereochemistry of Organometallic and Inorganic Compounds, Vol. V, Elsevier, New York, 1994, pp. 161–408.

[5] G. Nemra, P. Lemoine, P. Braunstein, C. de Méric de Bellefon, M. Ries, J. Organomet. Chem. 304 (1986) 245.

[6] (a) P. Braunstein, C. de Méric de Bellefon, M. Ries, J. Fischer, S.-E. Bouaoud, D. Grandjean, Inorg. Chem. 27 (1988) 1327. (b) P. Braunstein, C. de Méric de Bellefon, M. Ries, Inorg. Chem. 27 (1988) 1338.

[7] R. Uson, J. Fornies, P. Navarro, M. Tomas, C. Fortuño, J.I. Cebollado, A.J. Welch, Polyhedron 8 (1989) 1053.

[8] Such hypotheses concerning the direct and indirect components of a coupling through different pathways have been postulated for e.g. '$Pt_2(dppm)_2$' systems and $[Pt_3(CO)_3(PR_3)_3]$ clusters: (a) M.P. Brown, J.R. Fisher, S.J. Franklin, R.J. Puddephatt, K.R. Seddon, J. Organomet. Chem. 161 (1978) C46. (b) A. Moor, P.S. Pregosin, L.M. Venanzi, Inorg. Chem. Chim. Acta 48 (1981) 153.

[9] (a) J. Ellermann, F.A. Knoch, K.J. Meier, Z. Naturforsch., 45b (1990) 1657. (b) J. Ellermann, K.J. Meier, Z. Anorg. Allg. Chem. 603 (1991) 77.

[10] C.S. Browning, D.H. Farrar, D.C. Frankel, J.J. Vittal, Inorg. Chim. Acta 254 (1997) 329.

[11] (a) J. Ellermann, E.F. Hohenberger, W. Kehr, A. Purzer, G. Thiele, Z. Anorg. Allg. Chem. 464 (1980) 45. (b) J. Ellermann, L. Mader, Z. Naturforsch. Teil B 35 (1980) 307.

[12] U. Schubert, D. Neugebauer, A.A.M. Aly, Z. Anorg. Allg. Chem. 464 (1980) 217.

[13] D.E. Richardson, H. Taube, Inorg.Chem. 20 (1981) 1278.

[14] (a) V.W.-W. Yam, W.-K. Lee, K.-K. Cheung, B. Crystall, D. Philips, J. Chem. Soc. Dalton Trans. (1996) 3283. (b) V.W.-W. Yam, W.K.-M. Fung, M.-T. Wong, Organometallics 16 (1997) 1772.

[15] J.P. Lozos, B.M. Hoffman, C.G. Franz, QCPE 243 (1973) 11.

[16] S. Lo Schiavo, G. Bruno, P. Zanello, F. Laschi, P. Piraino, Inorg. Chem. 36 (1997) 1004.

[17] SADABS, Program for Siemens area detector absorption correction, G. Sheldrick, Institut fur Anorganische Chemie, Universitat Gottingen, 1996.